Assessment of corrosion-induced changes on the mechanical integrity of cemented carbides at small length scales

Y.F. Zheng, G. Fargas, H. Besharatloo, M. Serra, J.J. Roa, E. Armelin, O. Lavigne, L. Llanes

PII: S0263-4368(19)30520-7
DOI: https://doi.org/10.1016/j.ijrmhm.2019.105033
Article Number: 105033
Reference: RMHM 105033

To appear in: *International Journal of Refractory Metals and Hard Materials*

Received date: 2 July 2019
Revised date: 17 July 2019
Accepted date: 24 July 2019

Please cite this article as: Y.F. Zheng, G. Fargas, H. Besharatloo, et al., Assessment of corrosion-induced changes on the mechanical integrity of cemented carbides at small length scales, International Journal of Refractory Metals and Hard Materials, https://doi.org/10.1016/j.ijrmhm.2019.105033

Assessment of corrosion-induced changes on the mechanical integrity of cemented carbides at small length scales

Y. F. Zheng[a,b,*] yafeng.zheng@upc.edu, G. Fargas[a,b], H. Besharatloo[a,b], M. Serra[a], J. J. Roa[a,b], E. Armelin[b,c], O. Lavigne[d], L. Llanes[a,b]

[a]CIEFMA, Departament de Ciència dels Materials i Enginyeria Metal·lúrgica, EEBE, Universitat Politècnica de Catalunya, Barcelona 08019, Spain

[b]Barcelona Research Center in Multiscale Science and Engineering, Universitat Politècnica de Catalunya, Barcelona 08019, Spain

[c]IMEM, Departament d'Enginyeria Química, EEBE, Universitat Politècnica de Catalunya, Barcelona 08019, Spain

[d]Hyperion Materials & Technologies, 08107 Martorelles, Spain

[*]Corresponding author.

Abstract

In this work, the effect of corrosion-induced damage on the mechanical response of hardmetals was evaluated at small length-scale by means of nanoindentation and nanoscratch techniques. Damage was introduced in a controlled way through immersion of samples in acidic solution. It was found that surface degradation associated with corrosion leads to strong reduction of elastic modulus and hardness, as compared to non-corroded samples. Similarly, significant differences were observed in nanoscratch response, regarding not only the width and depth of tracks but also the deformation mechanisms developed as contact load is progressively increased. Damage emergence and evolution were evidenced in corroded surfaces at scratching loads significantly lower than for non-corroded specimens. Changes in nanoindentation and nanoscratch response and damage scenario are discussed on the basis of the effective microstructural assemblage remnant after corrosion action. In this regard, dissolution of metallic phase

becomes critical as it yields as a result a mechanically unsupported, contiguous and binderless/porous, carbide network. Consequently, cracking, fragmentation and easy removal of WC grains under contact loading is evidenced; and thus, mechanical integrity is effectively lessened.

Keywords: Cemented carbide; corrosion; nanoindentation; nanoscratch; small-scale mechanical integrity

1. Introduction

WC-Co cemented carbides, usually referred to as hardmetals, are found at the forefront of a wide range of engineering products that operate under harsh working conditions. Indeed, cemented carbides are the preferential choice in almost all the applications where the best solution against combined wear, impact and corrosion is sought [1]. The main reason behind it is the exceptional combination of intrinsic mechanical parameters (i.e. hardness and toughness), wear resistance and damage tolerance exhibited by them, as a result of the extremely different properties of their two interpenetrating constitutive phases: hard, brittle carbides and a soft, ductile metallic binder [2-4]. However, despite their outstanding properties, WC-Co alloys suffer from different degradation phenomena that seriously affect the performance and service-life of engineering structural parts. In this regard, many hardmetal applications involve exposure to chemically aggressive media, including a wide variety of corrosive environments such as lubricants, chemical and petrochemical products, and mine and sea waters, among others (e.g. Refs [5-9]).

Resistance to corrosion is not to be considered as a well-defined intrinsic material parameter; as it represents an observed qualitative performance which depends on various internal and external factors. From this perspective, the corrosion behavior of

hardmetals has been extensively investigated in recent decades using different testing methodologies and addressing influence of multiple factors, such as surface state, corrosive medium, microstructural assemblage and binder chemical nature [5-22]. In these studies, it has been shown that: (1) corrosive media preferentially attack the binder phase when exposed to acidic and neutral environments; (2) in alkaline solution, the Co binder exhibits a stable passivation, while the WC phase dissolves easily; (3) damage by corrosion induced by acidic media is usually much more pronounced than that of neutral and basic ones; and (4) a greater amount of dissolution of the binder phase in acid solution eventually results in the formation of the oxide layer of W and a region depleted in Co, compared to the exposure in neutral and basic solutions.

Optimal performance of engineering components is based on laboratory experiments attempting to simulate service-like conditions. Within this context, several studies have shown detrimental changes in the tribological response and effective wear resistance of cemented carbides as a result of the interaction among corrosion and other degradation phenomena such as erosion and abrasion [23-26]. Furthermore, relevant corrosion effects on residual strength, under imposed mechanical loads, have also been reported for hardmetals [27-32]. However, most of the above literature reports mainly address microstructure-medium-performance correlations from a macroscopic perspective, without in-depth analysis of damage micromechanisms involved. Interesting exceptions are the relatively recent works by Gee and coworkers [33-37] where degradation micromechanisms have been studied by implementing model abrasion tests, complemented with the use of advanced microscopic inspection techniques. This study attempts to follow an alike approach by evaluating corrosion effects on small-scale mechanical response of hardmetals. In this regard, nanoindentation and nanoscratch

techniques have been successfully implemented for determining mechanical and tribological properties of cemented carbides at micro- and nanometric length scales, as given by: (1) measurement of intrinsic hardness and elastic modulus of individual constituent phases [38-40]; (2) evaluation of microstructural effects on sliding contact, scratch and wear resistance [41-43]; and (3) documentation and analysis of deformation, wear and material removal mechanisms [39,40,42,43]. Unfortunately, all the referred works have been conducted on pristine or virgin hardmetals; hence, information on how the limit state – in terms of failure or acceptable/unacceptable criteria from a structural integrity viewpoint – is affected by the damage induced by corrosion is completely missing for cemented carbides. Within the above framework, it is the aim of this investigation to assess and analyze surface/subsurface and mechanical integrity changes induced by exposure to an acidic media of a hardmetal grade, by means of nanoindentation and nanoscratch testing complemented with combined use of Field Emission Scanning Electron Microscopy (FESEM) and Focused Ion Beam (FIB).

2. Experimental aspects

A plain WC-Co hardmetal grade was chosen for this study. It was supplied by Hyperion Materials and Technologies and is here referred to as 6CoM. Key microstructural parameters of the material investigated, including binder content ($\%_{wt.}$), mean grain size (d_{WC}), contiguity (C_{WC}) and binder mean free path (λ_{binder}), are listed in **Table 1**. Mean grain size was measured by the linear intercept method (LIM), using FESEM micrographs. Carbide contiguity and binder mean free path were estimated following empirical relationship given in the literature [3,44].

Corrosion damage was induced in a controlled way by immersing the hardmetal specimens in stirred 0.1M HCl solution at room temperature. A long exposure time (264

h) was selected, in order to obtain significant changes at both surface and subsurface levels. Before and after immersion tests, samples were hand-cleaned using soapy water, then ultrasonically cleaned for 15 min in ethanol, and finally dried in air. Corrosion effects were evaluated in terms of (1) existing phases, before and after immersion tests, by means of X-Ray diffraction (XRD) using Cu Kα (40 kV and 30 mA) radiation; and (2) microstructural changes discerned by cross-sectional inspection using optical microscopy (OM), laser scanning confocal microscopy (LSCM) and FESEM. The latter also allowed assessment of surface and subsurface integrity of corroded specimens.

Corrosion-induced changes on the mechanical properties were evaluated at small-length scale. Nanoindentation and nanoscratch tests were performed on both non-corroded (virgin and polished) and corroded surfaces using a Berkovich diamond indenter. Indentations were performed at a constant strain rate of 0.05 s^{-1}, up to the maximum displacement into surface or until reaching the maximum applied load of 650 mN. In these tests, hardness (*H*) and Young's modulus (*E*) were evaluated as a function of the penetration depth with a nanoindenter unit, according to Oliver and Pharr's model [45]. A homogeneous array of twenty-five indentations (5 by 5) were made on each sample and the results were averaged. Meanwhile, scratch tests were carried out under constant sliding contact rate (1 μm/s) while the indenter applied increasing loads as it moved along the scratch length. Tests were run until maximum load values of either 60 mN or 500 mN, along scratch lengths of 60 or 200 μm respectively.

Deformation and damage scenarios induced by residual imprints (nanoindentations) and tracks (nanoscratchs) were evaluated by inspecting contact surface and corresponding subsurface regions through a dual beam FESEM/Focused Ion Beam (FIB) unit.

Regarding cross-section examination, prior to milling, a thin protective layer of platinum was deposited on the region of interest to reduce waterfall effects, which affect the quality of the images. Current and acceleration voltage of Ga^+ source was subsequently reduced down to a final polishing stage at 500 pA at 30 kV respectively.

3. Results and discussion

3.1. Microstructural changes induced by corrosion

Figure 1 shows cross-sectional images obtained from OM and FESEM/FIB for the corroded specimen. They reveal a homogeneously degraded layer of about 450 µm in-depth (**Figure 1a**). As evidenced in **Figure 1b**, it is mainly the result of a preferential attack of cobalt binder which leads to a network of unsupported carbides throughout the affected layer. Such a finding is consistent with literature reports on the corrosion of WC-based hardmetals exposed to acidic media [15,17]. It is also in complete agreement with differences determined, before and after corrosion, in XRD patterns of the material studied. As it is discerned in **Figure 2**, cobalt peaks observed in the pristine specimens are absent after corrosion.

3.2. Nanoindentation tests: mechanical response and deformation/damage micromechanisms

Typical load-displacement (*P-h*) curves recorded from Berkovich indentation tests are given in **Figure 3**. It is clearly discerned that corrosion-induced damage has a significant effect on P-h behavior for the studied grade. It translates in an obvious increase (about 300 nm) of maximum penetration depth. **Figure 4** shows elastic modulus and hardness values as a function of penetration depth for both non-corroded and corroded surface conditions. Values are stabilised for penetration depths larger than 500 nm. At lower depths, measured values display considerable scatter due to scale effects (e.g. surface defects and roughness). Mechanical properties of the studied grade

are pronouncedly degraded due to the corrosion-induced damage. Young's modulus of 679 GPa and hardness of 24 GPa obtained for the virgin condition are in satisfactory agreement with those measured for similar grade at such small length scale. It then validates the much lower values determined for the corroded condition, 464 GPa and 15 GPa respectively, as a genuine effect of the corrosion-induced changes.

Deformation and damage scenario is also observed to change dramatically when comparing virgin and corroded specimens, as shown in **Figure 5**. For the non-corroded condition, as expected, both hard and soft phases exhibit effective deformation compatibility between them, with very few fracture features (cracks) localized in WC grains (**Figure 5a**). When subjected to mechanical loads, relatively high fracture toughness is beneficial for supressing and/or tolerating damage in structural materials. In cemented carbides, the metallic Co-base binder is able to deform by either mechanical twinning, dislocation slip and/or phase transformation [46-48]. Hence, most of the deformation imposed is absorbed for the metallic phase, avoiding then cracking of carbides. For the corroded specimen, the dissolution of the metallic binder reduces significantly load-bearing capability of the remnant microstructure, i.e. a mechanically unsupported carbide skeleton. This translates in easy removal of loose grains, as shown in **Figure 5b**.

Above ideas are further supported by FIB/FESEM cross-sectional inspection of residual imprints. As it is shown in **Figure 6**, the surface and mechanical integrity are significantly affected by corrosion. Different from the non-corroded specimen, where effective load-sharing between metal and ceramic phases is evidenced, the absence of the former in the corroded sample yields a completely distinct scenario. Here, the brittle

carbide phase must accommodate all the irreversible deformation imposed through direct load transfer between neighboring grains. As a result, local collapse of the unsupported (binderless and porous) carbide network and intensified multiple cracking is discerned.

3.3. Nanoscratch tests: mechanical response and deformation/damage micromechanisms

Scratch load-penetration depth curves resulting from nanoscratch testing are presented in **Figure 7**. As the load increases, both samples exhibit a rising penetration depth, as expected. Scratching penetration for a given applied load is significantly deeper for the corroded condition. This is consistent with the mechanical response recorded during nanoindentation. Under given nanoscratch condition, deeper penetration inevitably results in a larger damaged area, as it will be described later.

Figure 8 shows different post-scratch scenarios for both non-corroded and corroded conditions. In general, it is clearly discerned that failure-related events, i.e. spallation, cracking, etc., are much more pronounced in the corroded specimen. Virgin specimen exhibits a higher scratch resistance response, as concluded from the narrower and shallower tracks. This also applies to damage tolerance, as related to spallation and local chipping degree.

For non-corroded condition, a clear groove is discerned, where debris and some crushed particles are found to pile-up at the corresponding edges. This irreversible deformation and damage scenario is extremely more pronounced for the corroded condition, mainly as a result of a higher accumulation of the referred debris features. Thus, track edges are

rather ill-defined, although clearly linked to wider and deeper tracks, for a given applied load level.

Deformation and removal mechanisms along the scratch track were inspected in detail by means of FESEM. **Figure 9** illustrates that damage emerges earlier in the corroded specimen, as compared to the non-corroded one and in terms of applied load, i.e. ~ 45 mN and ~ 60 mN respectively. In the latter, changes are evidenced in terms of compatible plastic deformation between both phases as well as localized microfracture within contiguous carbide grains (**Figure 9a**). In this regard, the intrinsic toughening capability of the binder delays the generation of carbide microfracture and avoids potential grain pull-out [35,42]. Similar plastic deformation mechanisms are no longer discerned in scratch tracks for corroded specimens, regarding both metallic and ceramic phases. On the one hand, this finding is obvious as it is directly related to the absence of the metallic binder. On the other hand, it is the consequence of intensified stress at carbide/carbide contacts which then promotes fracture over plasticity within the hard phase. Finally, WC grains get severely fragmented and subsequently removed (**Figure 9b**).

Evolution of damage scenario with increasing imposed load for both non-corroded and corroded specimens is illustrated in **Figure 10**. It is seen that multiple and increasingly finer cracking of individual WC grains is also reached in the non-corroded specimen. However, different from the corroded case, WC fragments are then re-embedded into the deformed Co phase (**Figure 10a**), in agreement with wear mechanisms described in the literature [33-37,41,42,49,50]. In the corroded specimens, early fragmentation of individual carbide grains directly evolves into grain chipping, delamination and

dislodging (**Figure 10b**). At larger length scales, as applied load increases a rougher morphology, as well as a larger lump piling up near the groove edge, is also discerned.

In order to further document and understand the correlation between corrosion-induced damage and mechanical response degradation, a detailed cross-sectional inspection of scratch tracks was carried out by means of FIB/FESEM. **Figure 11** shows images corresponding to scratch tracks, at an applied load level of 225 mN, for non-corroded and corroded surfaces. Clearly, two-phase built-up material piled-up can be seen on the edge of the scratch track for the non-corroded surface. In contrast, edge tracks for the corroded specimens are characterized for large clumps of removed (and previously fragmented) carbide grains. As it has been discussed above, after binder dissolution, mechanical integrity of the remaining WC skeleton is significantly decreased; thus, loose grains can be easily removed even by light abrasion.

For the applied load level under consideration (225 mN), thickness of deformed zone discerned for the non-corroded specimen is around 2 μm (**Figure 11a**). Within such affected zone, deformation and fracture features are clearly discerned in both phases. When subjected to the compressive stresses induced by sliding contact (scratching), plastic deformation of Co binder first occurs close to interphase boundaries. As imposed stress rises, extrusion, cracking and removal of the binder phase (**Figures 11a-1** and **11a-2**) takes place. A further increase of stress induces WC microfracture and potential fragmentation of the individual grains. For the corroded specimens, strain energy associated with sliding contact is absorbed/released by means of two different deformation/fracture micromechanisms. On the one hand, loose WC grains near track edges are removed without further damage (e.g. cracking, chipping), as shown in

Figure 11b, due to lack of mechanical support. On the other hand, multiple cracking and fragmentation of individual carbides is extensively observed, as a direct consequence of load transfer through a contiguous and binderless (and porous) carbide network. Furthermore, some compaction of the open structure at the subsurface is also discerned by filling out of cavities with fragmented carbides as well as potential rotation and collapse of remnant carbide grains (**Figure 11b-1**).

4. Conclusions

Corrosion effects on microstructural assemblage, small-scale mechanical response (under contact loading) and involved deformation/fracture micromechanisms for a plain WC-Co hardmetal grade have been investigated. From the results presented in this study, the following conclusions may be drawn:

(1) Immersion testing in an acidic solution results in a significant degradation of surface /subsurface integrity of cemented carbides. In this regard, effective changes in microstructural assemblage of the material are discerned by FESEM/FIB inspection: from an interpenetrating two-phase network for the non-corroded composite to a contiguous and binderless (i.e. with cavities in regions where binder has been dissolved) carbide skeleton in the corroded material.

(2) Corrosion in acidic media is found to be quite detrimental for the mechanical integrity of the hardmetal alloy studied. Due to the lower load-bearing capability of the referred mechanically unsupported carbide network existing in the corroded cemented carbide, their elastic modulus, hardness and sliding contact (scratch) resistance are significantly degraded, as compared to those exhibited by the non-corroded hardmetal.

(3) Deformation/fracture micromechanisms are also significantly affected by corrosion. As the metallic binder is leached out during exposure to the acidic solution, its well-established toughening capability in non-corroded hardmetals is also completely lost. Consequently, deformation induced by the imposed loads must be exclusively accommodated by the binderless and porous network of carbide phase. It is done through multiple cracking and fragmentation of individual grains. Furthermore, as re-embedment of them into the metallic phase (as it occurs for the non-corroded specimens) is no longer possible, it finally yields easy pull-out and removal of the hard phase in the corroded material.

ACKNOWLEDGEMENTS

This work was financially supported by the collaborative Industry-University program between Hyperion Materials & Technologies and Universitat Politècnica de Catalunya, and partly funded by the Spanish Ministerio de Economía y Competividad through Grant MAT2015-70780-C4-3-P (MINECO/FEDER). Y. F. Zheng acknowledges the Ph.D. scholarship received from China Scholarship Council. J. J. Roa acknowledges the Serra Húnter programme of the Generalitat de Catalunya.

References

[1] L. Prakash, Fundamentals and general applications of hardmetals, in: V.K. Sarin, D. Mari, L. Llanes (Eds.) Comprehensive Hard Materials, Elsevier, UK, 2014: pp. 29-90. https://doi.org/10.1016/B978-0-08-096527-7.00002-7

[2] H. Exner, Physical and chemical nature of cemented carbides, Int. Met. Rev. 24 (1979) 149-173. https://doi.org/10.1179/imtr.1979.24.1.149

[3] B. Roebuck, E.A. Almond, Deformation and fracture processes and the physical metallurgy of WC-Co hardmetals, Int. Mater. Rev. 33 (1988) 90-110.
https://doi.org/10.1179/imr.1988.33.1.90

[4] E. Jiménez-Piqué, M. Turon-Vinas, H. Chen, T. Trifonov, J. Fair, E. Tarrés, L. Llanes, Focused ion beam tomography of WC-Co cemented carbides, Int. J. Refract. Met. Hard Mater. 67 (2017) 9-17.
https://doi.org/10.1016/j.ijrmhm.2017.04.007

[5] A.M. Human, H.E. Exner, The relationship between electrochemical behaviour and in-service corrosion of WC based cemented carbides, Int. J. Refract. Met. Hard Mater. 15 (1997) 65-71.
https://doi.org/10.1016/S0263-4368(96)00014-5

[6] B. Bozzini, G.P. De Gaudenzi, M. Serra, A. Fanigliulo, F. Bogani, Corrosion behaviour of WC- Co based hardmetal in neutral chloride and acid sulphate media, Mater. Corros. 53 (2002) 328-334.
https://doi.org/10.1002/1521-4176(200205)53:5<328::AID-MACO328>3.0.CO;2-G

[7] R. Lu, L. Minarro, Y.-Y. Su, R.M. Shemenski, Failure mechanism of cemented tungsten carbide dies in wet drawing process of steel cord filament, Int. J. Refract. Met. Hard Mater. 26 (2008) 589-600.
https://doi.org/10.1016/j.ijrmhm.2008.01.009

[8] Q. Zhang, Y. He, W. Wang, N. Lin, N. Li, Corrosion behavior of WC-Co hardmetals in the oil-in-water emulsions containing sulfate reducing Citrobacter sp., Corros. Sci. 94 (2015) 48-60.
https://doi.org/10.1016/j.corsci.2015.01.036

[9] B. Bozzini, B. Busson, G.P. De Gaudenzi, C. Humbert, A. Tadjeddine, Corrosion of cemented carbide grades in petrochemical slurries. Part I - Electrochemical adsorption

of CN^-, SCN^- and MBT: A study based on in situ SFG, Int. J. Refract. Met. Hard Mater. 60 (2016) 37-51.
https://doi.org/10.1016/j.ijrmhm.2016.06.010

[10] W.J. Tomlinson, C.R. Linzell, Anodic polarisation and corrosion of cemented carbides with cobalt and nickel binders, J. Mater. Sci. 23 (1988) 914-918.
https://doi.org/10.1007/BF01153988

[11] S. Sutthiruangwong, G. Mori, Corrosion properties of Co-based cemented carbides in acidic solutions, Int. J. Refract. Met. Hard Mater. 21 (2003) 135-145.
https://doi.org/10.1016/S0263-4368(03)00027-1

[12] B. Schnyder, C. Stössel-Sittig, R. Kötz, S. Hochstrasser-Kurz, H. Siegenthaler, Investigation of the electrochemical behaviour of WC-Co hardmetal with electrochemical and surface analytical methods, Surf. Sci. 566-568 (2004) 1240-1245.
https://doi.org/10.1016/j.susc.2004.06.102

[13] S. Sutthiruangwong, G. Mori, R. Kösters, Passivity and pseudopassivity of cemented carbides, Int. J. Refract. Met. Hard Mater. 23 (2005) 129-136.
https://doi.org/10.1016/j.ijrmhm.2004.11.006

[14] C. F. Barbatti, F. Sket, J. Garcia, A. Pyzalla, Influence of binder metal and surface treatment on the corrosion resistance of (W,Ti)C-based hardmetals, Surf. Coat. Technol. 201 (2006) 3314-3327.
https://doi.org/10.1016/j.surfcoat.2006.07.135

[15] S. Hochstrasser, Y.Mueller, C. Latkoczy, S. Virtanen, P. Schmutz, Analytical characterization of the corrosion mechanisms of WC-Co by electrochemical methods and inductively coupled plasma mass spectroscopy, Corros. Sci. 49 (2007) 2002-2020.
https://doi.org/10.1016/j.corsci.2006.08.022

[16] F.J.J. Kellner, H. Hildebrand, S. Virtanen, Effect of WC grain size on the corrosion behavior of WC-Co based hardmetals in alkaline solutions, Int. J. Refract. Met. Hard Mater. 27 (2009) 806-812.
https://doi.org/10.1016/j.ijrmhm.2009.02.004

[17] D.S. Konadu, J. Van der Merwe, J.H. Potgieter, S. Potgieter-Vermaak, C.N. Machio, The corrosion behaviour of WC-VC-Co hardmetals in acidic media, Corros. Sci. 52 (2010) 3118-3125.
https://doi.org/10.1016/j.corsci.2010.05.033

[18] Q. Zhang, N. Lin, Y. He, Effects of Mo additions on the corrosion behavior of WC-TiC-Ni hardmetals in acidic solutions, Int. J. Refract. Met. Hard Mater. 38 (2013) 15-25.
https://doi.org/10.1016/j.ijrmhm.2012.12.003

[19] N. Lin, Y. He, C. Wu, S. Liu, Y. Jiang, Influence of TiC additions on the corrosion behaviour of WC-Co hardmetals in alkaline solution, Int. J. Refract. Met. Hard Mater. 46 (2014) 52-57.
https://doi.org/10.1016/j.ijrmhm.2014.05.009

[20] L. Zhang, Y. Chen, Q.-L. Wan, T. Liu, W. Tian, Electrochemical corrosion behaviors of straight WC-Co alloys: Exclusive variation in grain sizes and aggressive media, Int. J. Refract. Met. Hard Mater. 57 (2016) 70-77.
https://doi.org/10.1016/j.ijrmhm.2016.02.009

[21] A.M. Ferro Rocha, A.C. Bastos, J.P. Cardoso, F. Rodrigues, M.G.S. Ferreira, Corrosion behaviour of WC hardmetals with nickel-based binders, Corros. Sci. 147 (2019) 384-393.
https://doi.org/10.1016/j.corsci.2018.11.015

[22] X. Zhang, J. Zhou, C. Liu, K. Li, N. Lin, Effects of Ni addition on mechanical properties and corrosion behaviors of coarse-grained WC-10(Co, Ni) cemented carbides Int. J. Refract. Met. Hard Mater. 80 (2019) 123-129. https://doi.org/10.1016/j.ijrmhm.2019.01.004

[23] H. Engqvist, U. Beste, N. Axén, The influence of pH on sliding wear of WC-based materials, Int. J. Refract. Met. Hard Mater. 18 (2000) 103-109. https://doi.org/10.1016/S0263-4368(00)00007-X

[24] A.J. Gant, M.G. Gee, A.T. May, The evaluation of tribo-corrosion synergy for WC-Co hardmetals in low stress abrasion, Wear 256 (2004) 500-516. https://doi.org/10.1016/j.wear.2003.04.001

[25] M. R. Thakare, J. A. Wharton, R. J. K. Wood, C. Menger, Exposure effects of alkaline drilling fluid on the microscale abrasion-corrosion of WC-based hardmetals, Wear 263 (2007) 125-136. https://doi.org/10.1016/j.wear.2006.12.047

[26] R.J.K. Wood, S. Herd, M.R. Thakare, A critical review of the tribocorrosion of cemented and thermal sprayed tungsten carbide, Tribol. Int. 119 (2018) 491-509. https://doi.org/10.1016/j.triboint.2017.10.006

[27] W.J. Tomlinson, I.D. Molyneux, Corrosion, erosion-corrosion, and the flexural strength of WC-Co hardmetals, J. Mater. Sci. 26 (1991) 1605-1608. https://doi.org/10.1007/BF00544670

[28] V.A. Pugsley, G. Korn, S. Luyckx, H.G. Sockel,W. Heinrich, M.Wolf, H. Feld, R. Schulte, The influence of a corrosive wood-cutting environment on the mechanical properties of hardmetal tools, Int. J. Refract. Met. Hard Mater. 19 (2001) 311-318. https://doi.org/10.1016/S0263-4368(01)00059-2

[29] V.A. Pugsley, H.-G. Sockel, Corrosion fatigue of cemented carbide cutting tool materials, Mater. Sci. Eng. A 366 (2004) 87-95.
https://doi.org/10.1016/j.msea.2003.08.057

[30] J.M. Tarragó, G. Fargas, E. Jimenez-Piqué, A. Felip, L. Isern, D. Coureaux, J.J. Roa, I. Al-Dawery, J. Fair, L. Llanes, Corrosion damage in WC-Co cemented carbides: residual strength assessment and 3D FIB-FESEM tomography characterisation, Powder Metall. 57 (2014) 324-330.
https://doi.org/10.1179/1743290114Y.0000000115

[31] J. M. Tarragó, G. Fargas, L. Isern, S. Dorvlo, L. Llanes, Microstructural influence on tolerance to corrosion-induced damage in hardmetals, Mater. Design 111 (2016) 36-43.
https://doi.org/10.1016/j.matdes.2016.08.066

[32] W. Tang, L. Zhang, Y. Chen, H. Zhang, L. Zhou, Corrosion and strength degradation behaviors of binderless WC material and WC-Co hardmetal in alkaline solution: A comparative investigation, Int. J. Refract. Met. Hard Mater. 68 (2017) 1-8.
https://doi.org/10.1016/j.ijrmhm.2017.06.003

[33] M.G. Gee, Model scratch corrosion studies for WC/Co hardmetals, Wear 268 (2010) 1170-1177.
https://doi.org/10.1016/j.wear.2010.01.004

[34] M.G. Gee, L. Nimishakavi, Model single point abrasion experiments on WC/Co hardmetals, Int. J. Refract. Met. Hard Mater. 29 (2011) 1-9.
https://doi.org/10.1016/j.ijrmhm.2010.04.009

[35] J.C.P. Zuñega, M.G. Gee, R.J.K. Wood, J. Walker, Scratch testing of WC/Co hardmetals, Tribol. Int. 54 (2012) 77-86.
https://doi.org/10.1016/j.triboint.2012.02.027

[36] A.J. Gant, M.G. Gee, D.D. Gohil, H.G. Jones, L.P. Orkney, Use of FIB/SEM to assess the tribo-corrosion of WC/Co hardmetals in model single point abrasion experiments, Tribol. Int. 68 (2013) 56-66.
https://doi.org/10.1016/j.triboint.2012.11.008

[37] M. Gee, K. Mingard, J. Nunn, B. Roebuck, A. Gant, In situ scratch testing and abrasion simulation of WC/Co. Int. J. Refract. Met. Hard Mater. 62 (2017) 192-201.
https://doi.org/10.1016/j.ijrmhm.2016.06.004

[38] M.G. Gee, B. Roebuck, P. Lindahl, H-O Andren, Constituent phase nanoindentation of WC/Co and Ti(C,N) hard metals, Mater. Sci. Eng. A209 (1996) 128-136.
https://doi.org/10.1016/0921-5093(95)10099-7

[39] A. Duszová, R. Halgaš, M. Bľanda, P. Hvizdoš, J. Morgiel, Nanoindentation of WC–Co hardmetals, J. Eur. Ceram. Soc. 33 (2013) 2227-2232.
https://doi.org/10.1016/j.jeurceramsoc.2012.12.018

[40] J. J. Roa, E. Jimenez-Pique, C. Verge, J. M. Tarragó, L. Llanes, Intrinsic hardness of constitutive phases in WC–Co composites: Nanoindentation testing, statistical analysis, WC crystal orientation effects and flow stress for the constrained metallic binder, J. Eur. Ceram. Soc. 35 (2015) 3419-3425.
https://doi.org/10.1016/j.jeurceramsoc.2015.04.021

[41] S. Ndlovu, K. Durst, M. Göken, Investigation of the sliding contact properties of WC-Co hard metals using nanoscratch testing, Wear 263 (2007) 1602-1609.
https://doi.org/10.1016/j.wear.2006.11.044

[42] H.Q. Sun, R. Irwan, H. Huang, G.W. Stachowiak, Surface characteristics and removal mechanism of cemented tungsten carbides in nanoscratching, Wear 268 (2010) 1400-1408.

https://doi.org/10.1016/j.wear.2010.02.014

[43] T. Csanádi, M. Novák, A. Naughton-Duszová, J. Dusza, Anisotropic nanoscratch resistance of WC grains in WC–Co composite, Int. J. Refract. Met. Hard Mater. 51 (2015) 188-191.

https://doi.org/10.1016/j.ijrmhm.2015.03.005

[44] J.M. Tarragó, D. Coureaux, Y. Torres, F. Yu, I. Al-Dawery, L. Llanes, Implementation of an effective time-saving two-stage methodology for microstructural characterization of cemented carbides, Int. J. Refract. Met. Hard Mater. 55 (2016) 80-86.

https://doi.org/10.1016/j.ijrmhm.2015.10.006

[45] W.C. Oliver, G.M. Pharr, An improved technique for determining hardness and elastic modulus using load and displacement sensing indentation experiments, J. Mater. Res. 7 (1992) 1564-1583.

https://doi.org/10.1557/JMR.1992.1564

[46] V.K. Sarin, T. Johannesson, On the deformation of WC-Co cemented carbides, Meter. Sci. 9 (1975) 472-476.

https://doi.org/10.1179/030634575790444531

[47] B. Roebuck, E.A. Almond, The influence of composition, phase transformation and varying the relative F.C.C. and H.C.P. phase contents on the properties of dilute Co-W-C Alloys, Mater. Sci. Eng. A 66 (1984) 179-194.

https://doi.org/10.1016/0025-5416(84)90179-4

[48] C. H. Vasel, A. D. Krawitz, E. F. Drake, E. A. Kenik, Binder deformation in WC-(Co,Ni) cemented carbide composites, Metall. Mater. Trans. A 16 (1985) 2309-2317.

https://doi.org/10.1007/BF02670431

[49] M. Gee, A. Gant, B. Roebuck, Wear mechanisms in abrasion and erosion of WC/Co and related hardmetals, Wear 263 (2007) 137-148.
https://doi.org/10.1016/j.wear.2006.12.046

[50] J. Heinrichs, M. Olsson, S. Jacobson, Surface degradation of cemented carbides in scratching contact with granite and diamond-the roles of microstructure and composition, Wear 342 (2015) 210-221.
https://doi.org/10.1016/j.wear.2015.08.024

List of tables

Table 1. Microstructural parameters for the investigated cemented carbide.

wt.% Co	d_{WC} (μm)	C_{WC}	λ_{binder} (μm)
6	1.51±0.16	0.48±0.02	0.32±0.03

List of figures

Figure 7. Typical penetration depth - scratch distance (under increasing applied load condition) curves obtained for uncorroded and corroded specimens.

Figure 8. LSCM micrographs of two scratch tracks performed on **(a)** non-corroded and **(b)** corroded samples.

Figure 9. FESEM images showing early damage features along the scratch track in **(a)** non-corroded and **(b)** corroded samples.

Figure 10. Scratch track view associated with three different applied load levels: 125 mN, 250 mN and 375 mN, for **(a)** non-corroded and **(b)** corroded surfaces.

Figure 11. FIB cross-sections of the scratch track corresponding to a load level of 225 mN in **(a)** non-corroded and **(b)** corroded surfaces.

Figure 1. Cross-section images illustrating **(a)** microscopic aspect and **(b)** microstructural changes of degraded layer, resulting after immersion in 0.1M HCl solution for 264 h of the hardmetal grade studied.

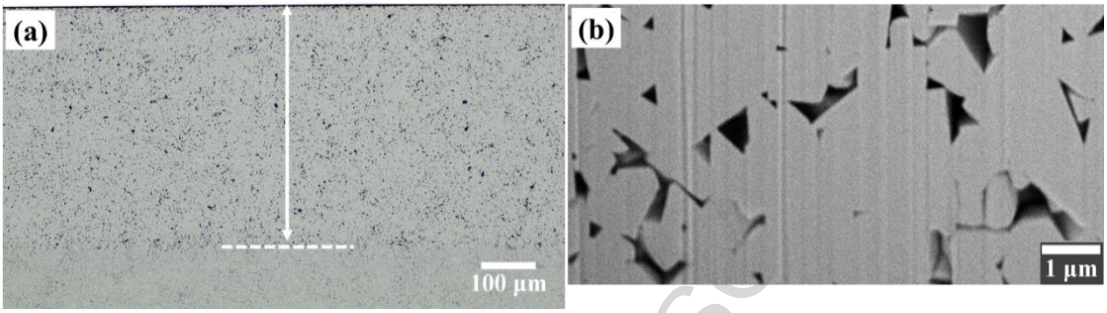

Figure 2. XRD patterns determined for the alloy studied: **(a)** before, and **(b)** after immersion test.

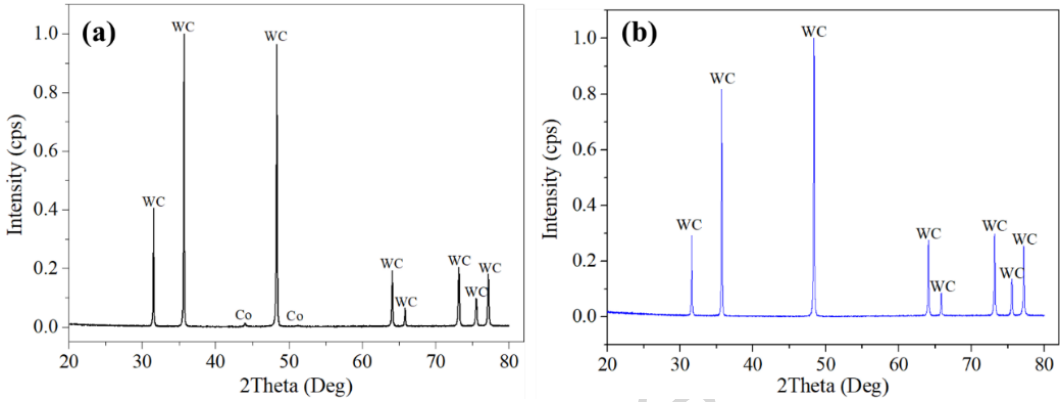

Figure 3. Representative indentation *P-h* curves from Berkovich indentation for both surface conditions studied.

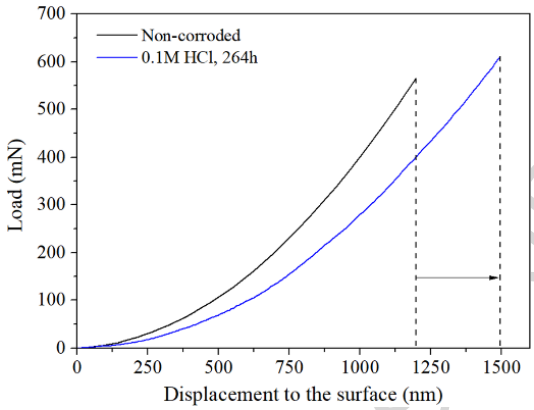

Figure 4. (a) Young's modulus and **(b)** hardness values as a function of penetration depth for non-corroded (black) and corroded (blue) samples.

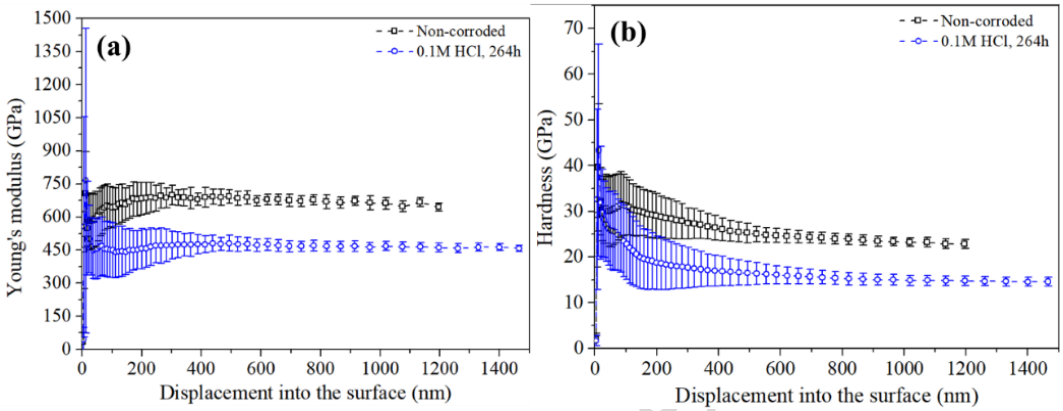

Figure 5. Residual imprints obtained as a result of nanoindenting (up to maximum displacement into surface of 2000 nm) **(a)** non-corroded and **(b)** corroded surfaces.

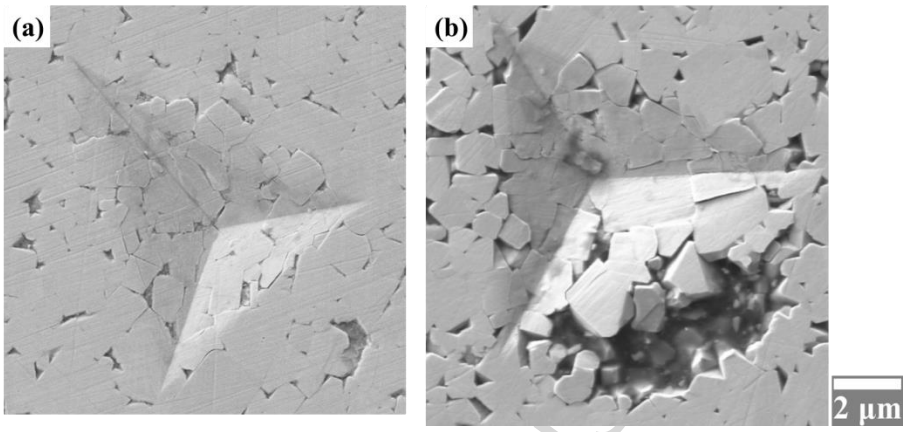

Figure 6. FIB cross-section of a Berkovich indented surface: **(a)** non-corroded and **(b)** corroded 6CoM.

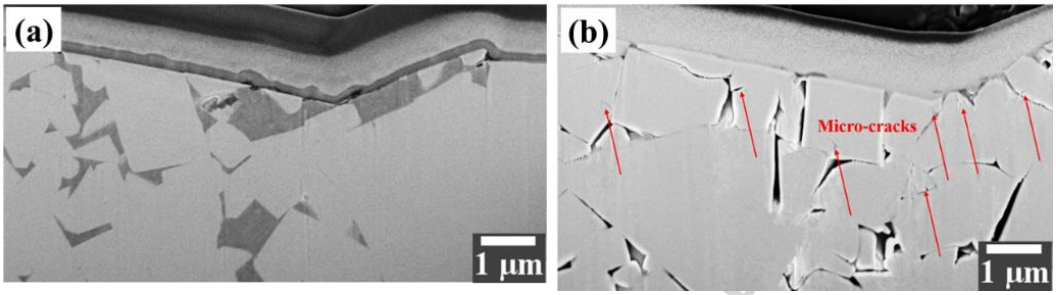

Figure 7. Typical penetration depth - scratch distance (under increasing applied load condition) curves obtained for uncorroded and corroded specimens.

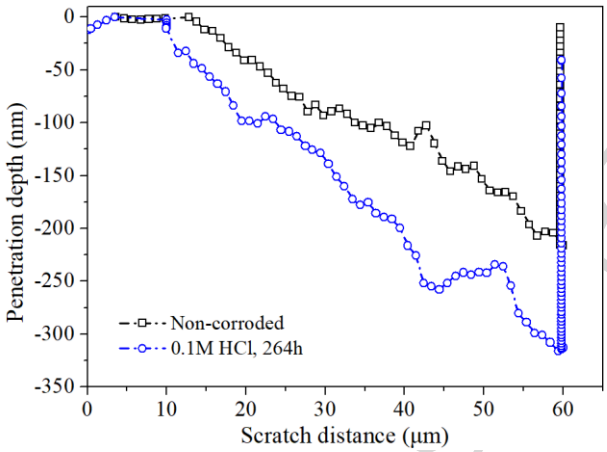

Figure 8. LSCM micrographs of two scratch tracks performed on **(a)** non-corroded and **(b)** corroded samples.

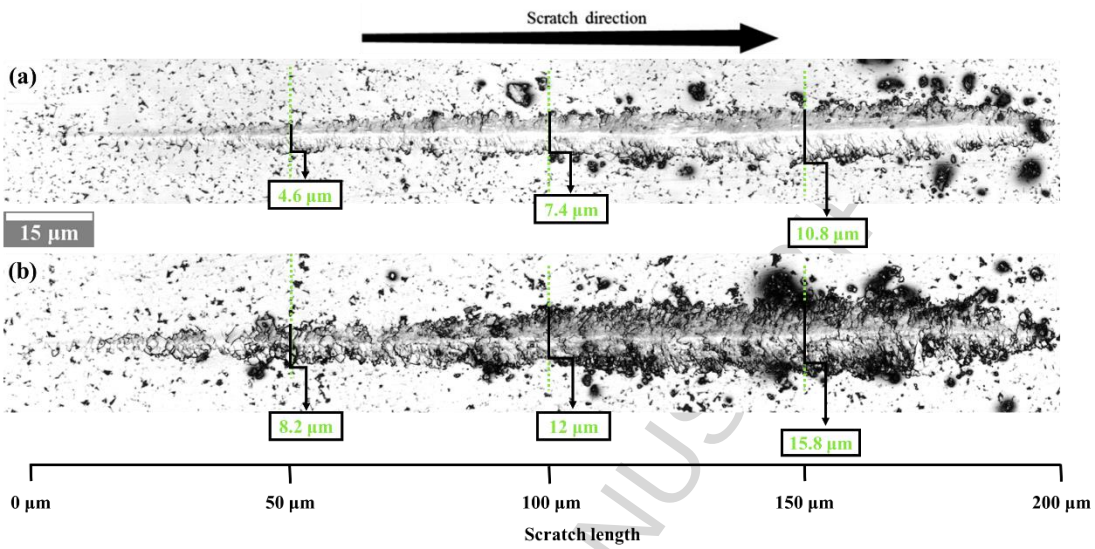

Figure 9. FESEM images showing early damage features along the scratch track in **(a)** non-corroded and **(b)** corroded samples.

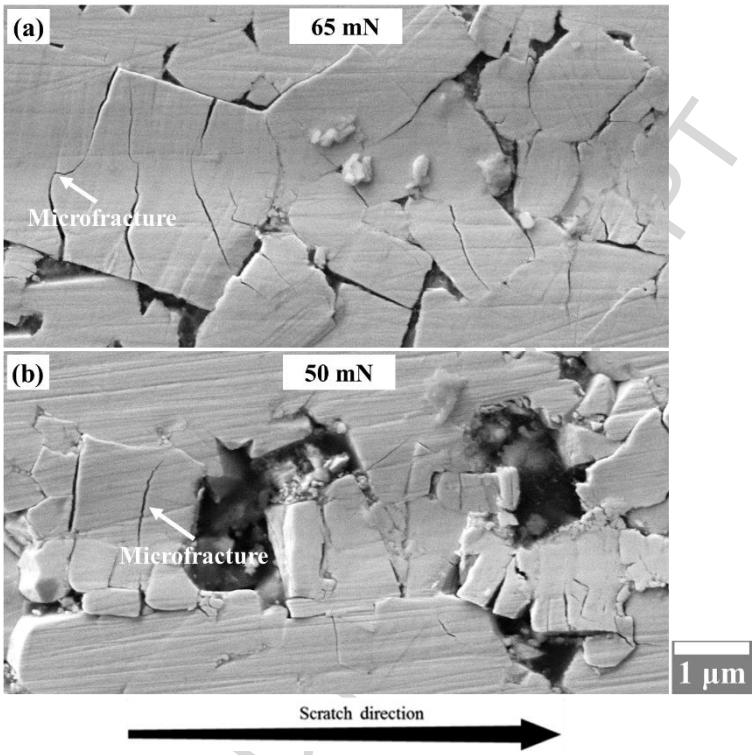

Figure 10. Scratch track view associated with three different applied load levels: 125 mN, 250 mN and 375 mN, for **(a)** non-corroded and **(b)** corroded surfaces.

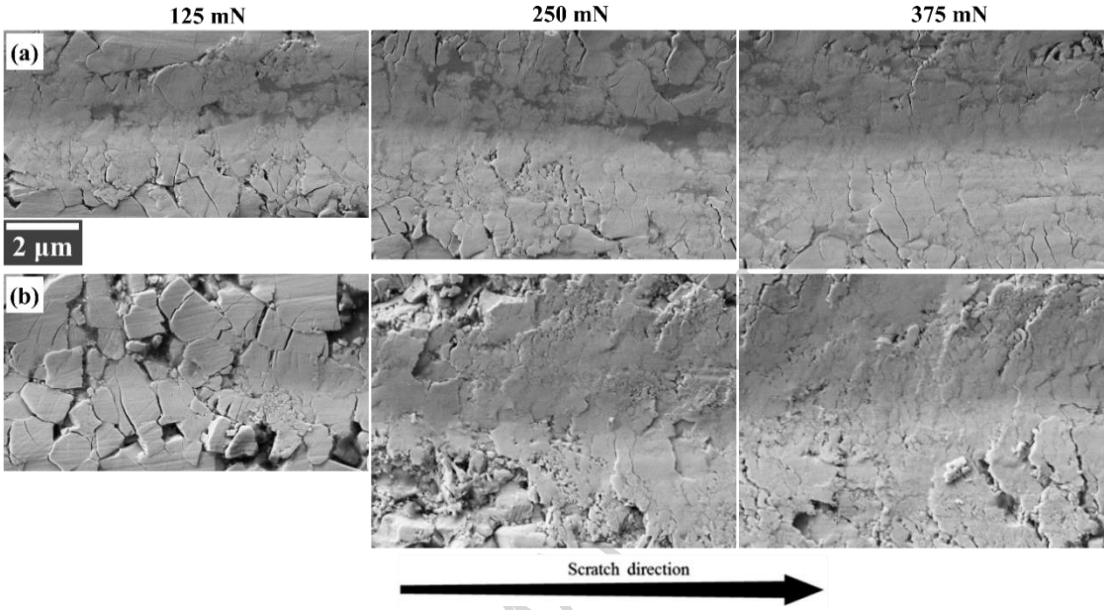

Figure 11. FIB cross-sections of the scratch track corresponding to a load level of 225 mN in **(a)** non-corroded and **(b)** corroded surfaces.

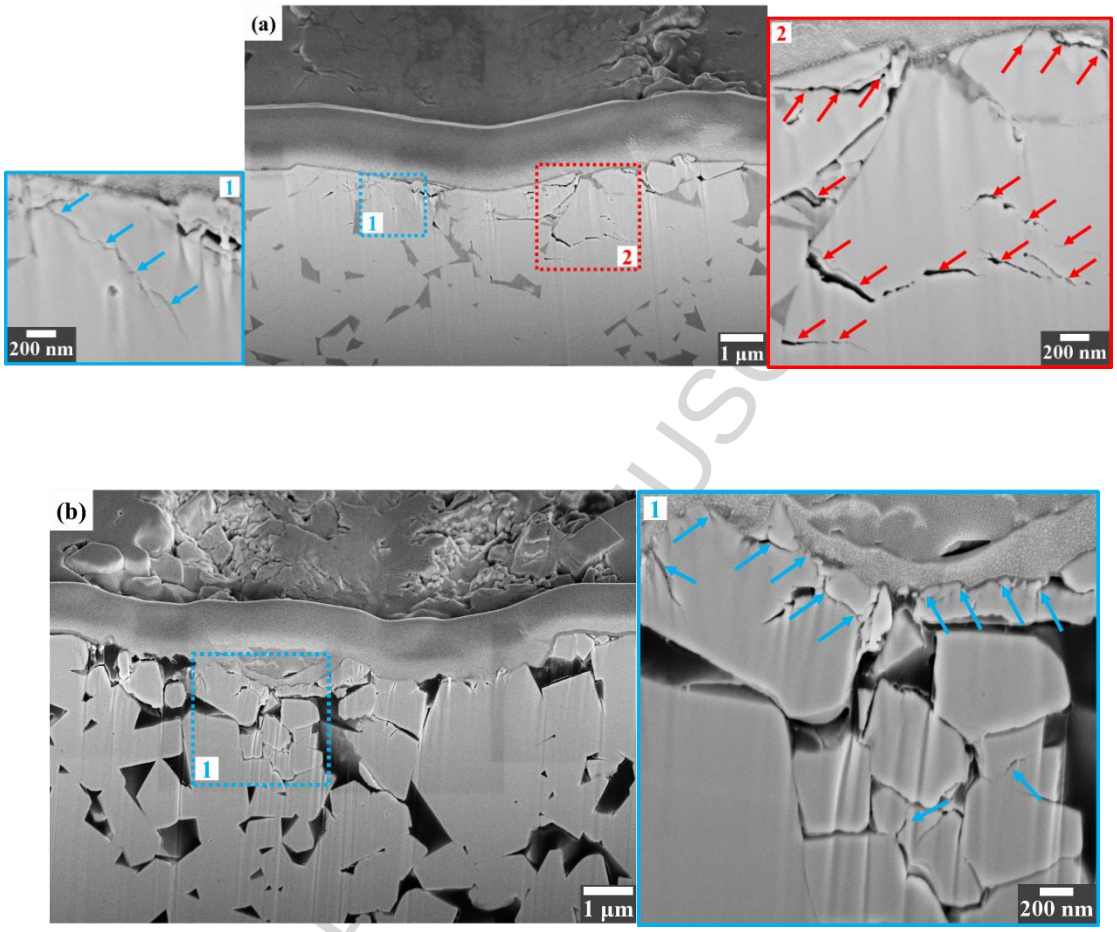

Highlights

Influence of corrosion-induced damage on the small length-scale mechanical response of hardmetals is studied

Significant changes are evidenced in nanoindentation and nanoscratch response of corroded cemented carbides

Lessening of mechanical integrity is due to effective microstructural assemblage remnant after corrosion action.

Dissolution of metallic phase becomes critical as it yields as a result a mechanically unsupported, contiguous and binderless/porous, carbide network.